

Article

Study on Modified Water Glass Used in High Temperature Protective Glass Coating for Ti-6Al-4V Titanium Alloy

Shuang Yang ¹ , Dali Zhou ^{1,*}, Jiabei Zhou ¹, Lei Yang ¹, Qing Fan ¹, Qianqian Yao ¹ and Yongqiang Yang ²

¹ College of Materials Science and Engineering, Sichuan University, Chengdu 610064, China; shone_yang@163.com (S.Y.); zjb@scu.edu.cn (J.Z.); lyang1986@scu.edu.cn (L.Y.); fanqing_scu@163.com (Q.F.); qqian0207@163.com (Q.Y.)

² Southwest Institute of Technical Physics, Chengdu 610041, China; yangyongqiang1376@163.com

* Correspondence: zdl@scu.edu.cn; Tel.: +86-28-8541-0272

Received: 27 February 2018; Accepted: 19 April 2018; Published: 26 April 2018



Abstract: Sodium silicate water glass was modified with sodium polyacrylate as the binder, the composite slurry used for high-temperature oxidation-resistant coating was prepared by mixing glass powder with good lubrication properties in the binder. The properties of the modified binder and high-temperature oxidation resistance of Ti-6Al-4V titanium alloy coated with composite glass coating were studied by XRD, SEM, EDS, TG-DSC and so on. Results showed that sodium polyacrylate modified water glass could obviously improve the suspension stability of the binder, the pyrolytic carbon in the binder at high temperature could increase the surface tension in the molten glass system, and the composite glass coating could be smooth and dense after heating. Pyrolytic carbon diffused and combined with oxygen in the coating under the heating process to protect the titanium alloy from oxidation. The thickness of the oxide layer was reduced 51% after applying the high-temperature oxidation-resistant coating. The coating also showed a nearly 30% reduction in friction coefficient due to the boundary lubricant regime. During cooling, the coating could be peeled off easily because of the mismatched CTE between the coating and substrate.

Keywords: sodium silicate water glass; sodium polyacrylate; titanium alloy; coating; oxidation resistant; lubricant

1. Introduction

Titanium alloy is widely used in aviation, navigation, and biomedical engineering due to its high strength, low density, and excellent corrosion resistance. Ti-6Al-4V titanium alloy is one of the most common titanium alloys. Ti-6Al-4V titanium alloy is difficult to be shaped at room temperature, and structural components are always made by using hot forging, hot extrusion, hot spinning, etc. [1,2]. However, effective oxidation protection of titanium alloy is an urgent problem to be solved [3,4]. The molding temperature of Ti-6Al-4V titanium alloy is 850–950 °C, and high-temperature oxidation protection technology of the alloy should be carefully investigated. In the metal-forming process at high temperatures, friction plays a significant role on the quality of finished product, life of tools, and formability of materials [5]. Thus, studying the friction and wear resistance of Ti-6Al-4V titanium alloy is very necessary.

In recent years, glass-ceramic coatings have become very promising materials for the protection against titanium alloy oxidation at elevated temperatures due to excellent chemical inertness, self-healing ability, and high-temperature stability [6–8]. Moreover, the slurry-dipping method is

a simple way which makes a more convenient and cheap preparation method for the application of coatings.

Glass-ceramic coatings mixed with liquid binder can offer remarkable protection for the alloy during heat treatment [9,10]. At elevated temperature, the coating materials fuse to form a strong adherent coating; otherwise, cracks appear easily. The coating is abandoned easily without heat treatment. Alcohol-based binders [11,12] have a low ability to suspend powders, so a satisfying stability of suspension is not available. Alumina sol [13], silica sol [14], and water glass are commonly used as inorganic binders. Alumina and silica sol have strong trends to gel. Therefore, it is not conducive for the storage of a coating. Water glass can meet some criteria, including high wetting ability to alloys and medium viscosity at high temperature, applicability, and cost-effectiveness. Sodium water glass (water glass = WG) ($\text{Na}_2\text{O}\cdot n\text{SiO}_2$) and potassium water glass are the most common water glasses in daily life [5,15]. However, coatings with water glass have low abilities to suspend powders. Despite the disadvantages of water glass, limited research has been carried on the performance improvement of water glass.

In this work, sodium polyacrylate (PAANa)-modified sodium water glass (modified sodium water glass = MWG) as a new organic-inorganic binder was investigated. A glass coating with this kind of modified binder was deposited on Ti-6Al-4V titanium alloy by using the slurry-dipping method.

2. Materials and Methods

The investigations in this work were performed on Ti-6Al-4V titanium alloy (chemical composition: Ti-6Al-4V-0.2Fe-0.05Si-0.08C-0.015H-0.05N, wt %). The specimen size was 20 mm \times 10 mm \times 10 mm. The specimen was ground on #200 SiC abrasive papers to remove the oxide layer of the alloy, subsequently cleaned with acetone in an ultrasonic bath, and then dried at 60 °C.

Table 1 shows the chemical composition of the glass powder used in this work, the required raw materials in powder form were mixed and heated in a high-temperature furnace at 1500 °C for 2 h in air, and then the molten glass was quenched in water. The molten glass exploded into fragments in the water. The fragments were ball-milled with water for 1 h. The slurry was dried and passed through the 200 mesh sieve to obtain a fine powder (powder size < 74 μm). The softening temperature (T_f) of the glass is 760 °C, so the glass powder can melt into liquid at 850 °C.

Table 1. Chemical composition (wt %) of glass powder.

SiO ₂	B ₂ O ₃	Al ₂ O ₃	CaO	MgO	Na ₂ O	BaO
62	10	2	4	4	14	4

Table 2 showed the composition of sodium water glass and modified sodium water glass used in this work. The water glass used in this study was commercially available. Water glass was made by melting alkali oxide and silica together, and then adding water in an autoclave at 130 °C to 170 °C. The purity of the water glass in the article is 98%. The viscosity of the water glass solution at temperature can be easily changed by adding any volume of water. Alkali oxide used in this work is Na₂O, and the molar ratio of SiO₂/Na₂O is 2.5. First, sodium water glass was added to the water. PAANa powder was added slowly with rapid stirring for 10 min. The entire solution was allowed to homogenize for 4 h until all the PAANa dissolved.

Table 2. Compositions (wt %) of the modified binders.

Component	PAANa	Sodium Water Glass	H ₂ O
WG	0	30	70
MWG	0.5	30	69.5

A slurry (glass powder dispersed in binder, solid content 50 wt %) was deposited on the Ti-6Al-4V alloy and dried in a natural environment. The investigations of the coating morphologies were carried out by using a scanning electron microscope (SEM) (MERLIN Compact, Zeiss, Oberkochen, Germany).

To evaluate the oxidation-resistant effect of coatings on Ti-6Al-4V alloy at high temperature, the bare and coated specimens were heated at 850 °C for 2 h in a muffle furnace under an air atmosphere. The coating materials fused to form a strong adherent coating during the heat treatment. Then specimens were cooled to room temperature in air after heating. The oxide layer (OL) of the specimens was investigated by using an energy-dispersive X-ray spectroscopy (EDS) (Inca X-Max, Oxford Instruments, Oxford, UK).

The modified binder solution was heated at 100 °C for 24 h to completely become a gel state. Investigations of the modified binder were carried out by using a scanning electron microscope (SEM) (MERLIN Compact, Zeiss, Oberkochen, Germany). The thermal behavior of the modified binder was analyzed through thermogravimetry-differential scanning calorimetry (TG-DSC) (STA449F3, NETZSCH, Free State of Bavaria, Germany). Scans were recorded from 50 °C to 950 °C in air at a heating rate of 10 °C/min.

Phase identification of the modified binders was carried out by using X-ray diffraction (XRD) (XRD-6100, SHIMADZU, Tokyo, Japan). The XRD patterns were recorded with Cu K α radiation of $\lambda = 0.15406$ nm on plan-view specimens from 10° to 100°. The scan speed was 4°/min and the step size was 0.02°.

The friction and wear resistance of Si₃N₄/Ti-6Al-4V contact were determined by a ball-on-disk tribotester (UMT-3) (BRUKER, Berlin, Germany) under unlubricated and lubricated conditions, respectively. The lubricant was the slurry mixed with glass powder and MWG. A pre-cleaned 5 mm Si₃N₄ ball with an average surface roughness of -200 nm was used as the counter surface. The testing conditions were as follows: an applied load of 10 N equal to 1.37 GPa of the maximum Hertz contact stresses, a linear velocity of 0.05 ms⁻¹, and a temperature of 850 °C.

3. Results

3.1. Surface Morphologies of MWG

The viscosity of the WG solution is not much different with water. However, its viscosity increases significantly after adding PAANa. PAANa ($-\text{CH}_2\text{COONa}-$) is an anionic polyelectrolyte, it can be dissociated into negative charge ($-\text{COO}^-$) and positive charge (Na^+) in water. The long molecular chain of PAANa is negatively charged. As a result, the chain extends to a long chain because of electrostatic repulsion. Thus, the viscosity of the MWG binder increases [16,17]. Surface morphologies of the MWG binder dried at room temperature are shown in Figure 1. With the addition of sodium water glass, the concentration of Na^+ increases, Na^+ combines with $-\text{COO}^-$ in the PAANa, and the long molecular chain is divided into many short sticks. Thus, the irregular stick structure is formed and the viscosity of the liquid decreases. Three different structures are shown in Figure 1: the stick organization, the clean surface, and small particles (areas marked as A, B, and C in Figure 1). The EDS results of the chemical composition of the areas marked as A–C in Figure 1 are presented in Table 3. The elemental contents of the clean surface (B) and small particles (C) are basically consistent, the ratio of sodium and silicon is about 1.7. This result demonstrates that the small particles are separated out from the clean surface. The ratio of sodium and silicon in area A is 2.6, which is much higher than that of area B and area C. However, there is little difference in the content of silicon in the three areas; obviously, the content of sodium in area A is higher. This demonstrates that Na^+ aggregates to a great degree due to the addition of sodium water glass, and according to the neutralization reaction, $-\text{COO}^-$ combines with Na^+ . Then the morphology of the binder surfaces are changed from long chains to the stick organization. A large number of short chains exist in the MWG binder with a large number of negative charges, and the effect of electrostatic repulsion can make the slurry suspend well. Testing shows that

the Zeta potential for the MWG binder was -47 mV; by contrast the Zeta potential for WG binder was -17 mV. The MWG binder has good suspension stability.

Table 3. Chemical composition (wt %) of the WMG binder via EDS.

No.	A	B	C
Na	27.79	17.88	21.35
Si	10.52	10.41	12.55

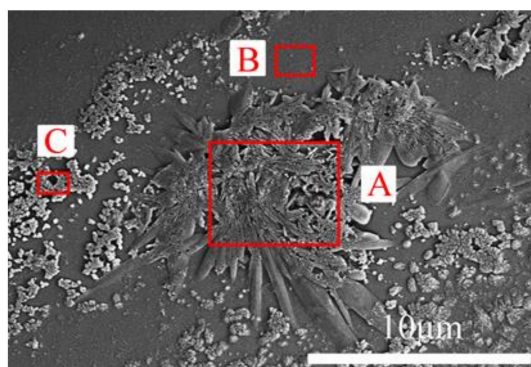


Figure 1. Surface morphology of the MWG binder at room temperature. Areas marked as A, B, and C, respectively.

3.2. Phase Composition of MWG

XRD patterns of the MWG binder under different temperatures with different times are given in Figure 2. The presence of $\text{Na}_2\text{SiO}_3 \cdot 9\text{H}_2\text{O}$, $\text{Na}_2\text{Si}_3\text{O}_7$, HCOONa , and SiO_2 are revealed from 100 °C to 300 °C, together with amorphous phase at 25° to 35° . The presence of an amorphous phase can be attributed to the random arrangement of the water glass. The $\beta\text{-Na}_2\text{Si}_2\text{O}_5$ with poor crystallinity is observed at 400 °C. From 500 °C to 600 °C, The $\beta\text{-Na}_2\text{Si}_2\text{O}_5$ is crystallized well. When the temperature increases to 700 °C, the phase changes into $\alpha_{\text{III}}\text{-Na}_2\text{Si}_2\text{O}_5$. Depending on the different temperatures and pressures, there are eight kinds of crystal forms [18]. The structures for all kinds of $\text{Na}_2\text{Si}_2\text{O}_5$ are lamellar. A six-membered ring is formed by a layer of $[\text{SiO}_4]$ tetrahedron, and Na^+ combines with a non-bridge oxygen of the $[\text{SiO}_4]$ tetrahedron. Free Na^+ can combine with the $[\text{SiO}_4]$ tetrahedron to form a remote-ordered crystal structure at $400\text{--}700$ °C. Sodium water glass returns to an amorphous state when the temperature increases to 800 °C. The melting point (T_m) of sodium water glass is 1100 °C, and the phase transition point (T_g) is 805 °C. $T_m/T_g > 2/3$, showing that the sodium water glass easily obtains an amorphous structure.

3.3. Thermal Behavior of MWG and PAANa

The thermal behavior and stability property of MWG binder and PAANa at high temperatures are shown in Figure 3. The total weight loss of MWG binder is 21.85% (relatively low). The TG-DSC curve can be divided into three main stages. At the first stage, the branched chains ($-\text{COO}^-$) and internal water of the MWG binder are lost when the temperature increases from 100 °C to 400 °C. This phenomenon is also confirmed by the XRD patterns of the MWG binder (Figure 2), and HCOONa is lost at 500 °C. A very large exothermic peak is shown at 445.6 °C in the second stage. The result is attributed to the fracture of the main carbon-carbon chain. The weight loss slows down at the third stage (after 450 °C). Phase splitting phenomenon happened in the MWG binder at 530 °C, and cristobalite is generated, so there is an endothermic peak [19]. Combined with XRD patterns of Figure 2, the phase of the MWG binder is changed from a crystalline phase to an amorphous phase at 800 °C. Thus, a large quantity of heat is absorbed by the water glass. Even though the content

of PAANa in the MWG binder is only 0.5%, the exothermic peak produced by the oxidation of the pyrolysis carbon is covered. After 800 °C, pyrolysis carbon in the second stage begins to be oxidized (Figure 3b). Overall, the MWG binder can sustain a relatively low consumption and exhibit good stability after 700 °C, which is beneficial to oxidation resistance at high temperatures.

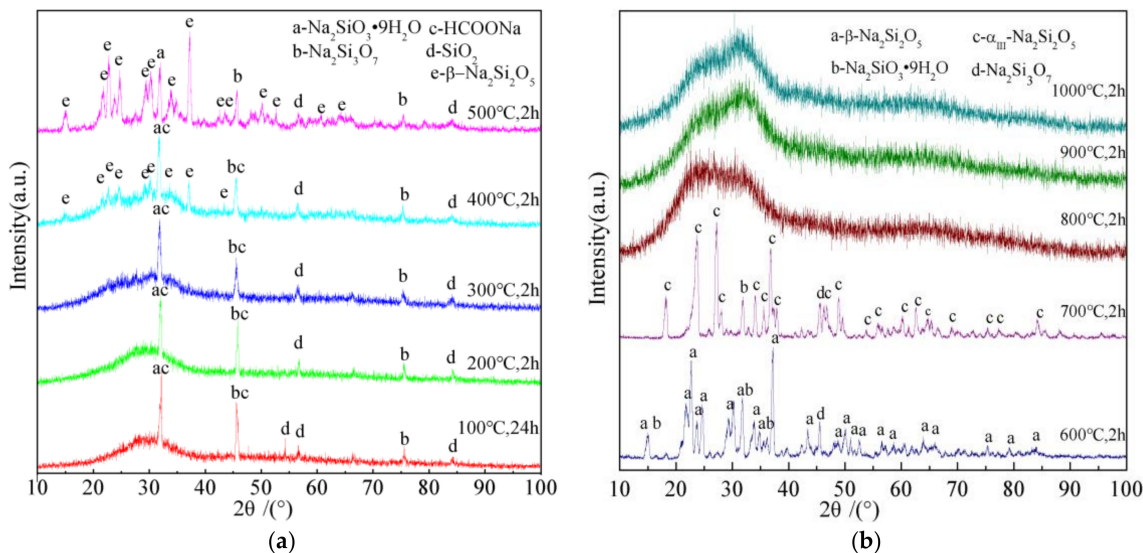


Figure 2. XRD patterns of the MWG binder under different temperatures with different times: (a) XRD patterns of the MWG binder at 100 °C for 24 h and between 200 °C to 500 °C for 2 h; and (b) XRD patterns of the MWG binder between 600 °C to 1000 °C for 2 h.

The TG curve of PAANa is shown in Figure 3b. The TG curve can also be divided into three stages. At the early stage, the branched chains ($-\text{COO}^-$) were lost with the temperature ranging from 100 °C to 420 °C. This phenomenon is also confirmed by the XRD patterns of the MWG binder, HCOONa was lost at 500 °C. At the second stage, weight loss is attributed to the fracture of the main carbon-carbon. At the third stage, pyrolysis carbon in the second stage began to oxidize at 800 °C.

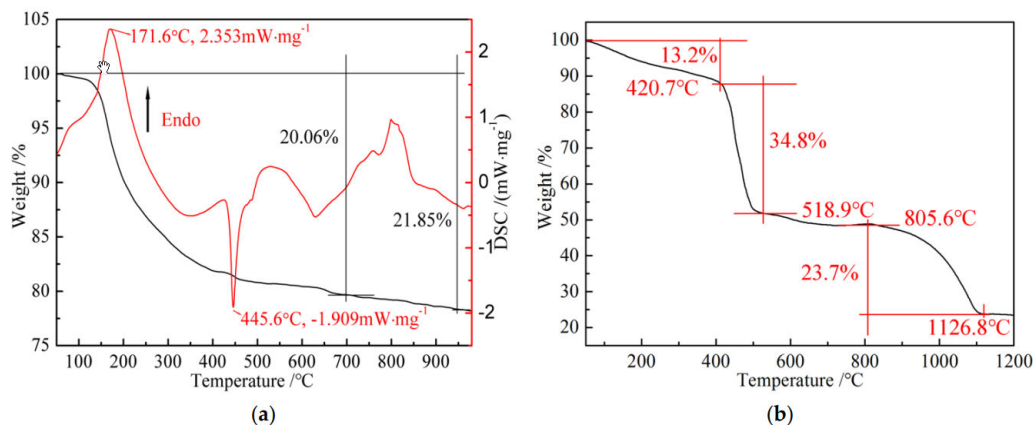


Figure 3. (a) The TG-DSC curve of the MWG binder; (b) The TG-curve of PAANa.

3.4. Oxidation Resistance of Ti-6Al-4V

Glass composite coating could be brought to a viscous liquid at high temperature. In this case, volatility and weight loss are inevitable, and the method of weight gain measurement causes uncertainties in the accuracy of the test results to some extent. Therefore, oxidation resistance was characterized by using EDS mapping in this study.

The cross-sectional SEM images and EDS mapping of bare alloy at 850 °C for 2 h are shown in Figure 4. As shown in the figure, extensive oxidation is observed for the bare alloy after exposure. The thickness of the oxide layer is approximately 82 μm . During the oxidation process, oxygen partial pressure reduces the minimum activity of Al_2O_3 between the air and the oxide layer at the interface. Al diffused from the inner area to the surface. Even though the content of Al is not sufficient to form an Al_2O_3 layer, there is some Al_2O_3 underneath the TiO_2 layer after oxidation. The oxide layer is porous and brittle, and oxygen easily diffuses through the substrate. Thus, oxygen can easily combine with titanium to become a solid solution.

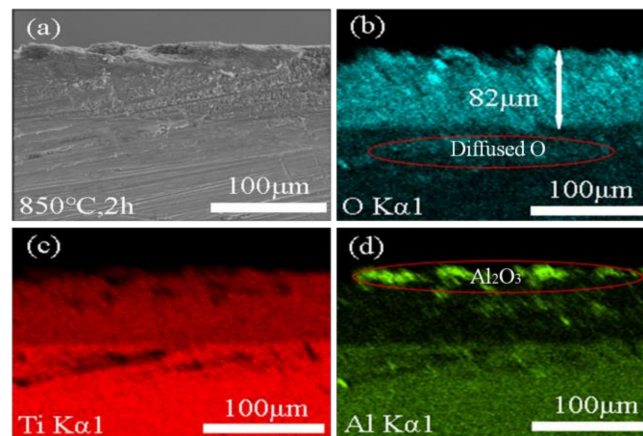


Figure 4. Cross-section of bare titanium alloy after oxidation at 850 °C for 2 h. (a) cross-sectional SEM image; (b) O element distribution at EDS mapping image; (c) Ti element distribution at EDS mapping image; (d) Al element distribution at EDS mapping image.

The thickness of oxide layer with coated specimen prepared by MWG binder (Figure 5) is 42 μm . This result indicates that good protection is offered by this kind of coating, and PAANA does not have any negative effect on the oxidation resistance of the coating. Diffusion phenomenon occurs at high temperature between the coating and oxide layer. With a strong combination between the coating and oxide layer, coating is not easily squeezed out under the hot forming process.

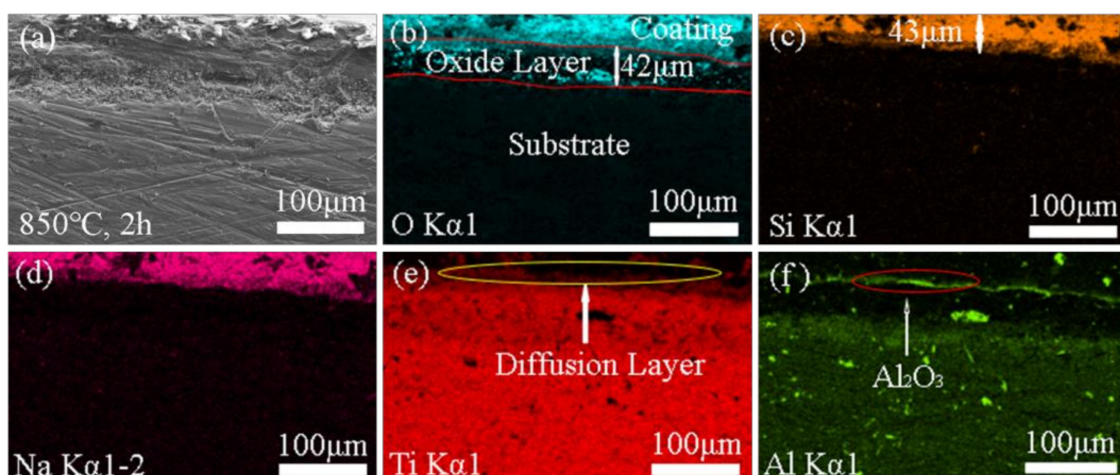
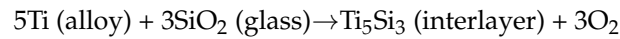


Figure 5. Cross-section of the coated specimen prepared by the MWG binder after oxidation at 850 °C for 2 h. (a) cross-sectional SEM image; (b) O element distribution at EDS mapping image; (c) Si element distribution at EDS mapping image; (d) Na element distribution at EDS mapping image; (e) Ti element distribution at EDS mapping image; and (f) Al element distribution at EDS mapping image.

Surface morphologies of two kinds of glass composite coating after heating at 850 °C for 2 h are shown in Figure 6. These two kinds of coating are prepared with WG binder and MWG binder, respectively. From Figure 6a, a large number of pores can be observed on the coating, however, the coating surface shown in Figure 6b is bright and clean. The pores in the glass coating are formed by the oxygen produced by the reaction between the coating and the titanium base [6]:



The pyrolysis carbon decomposed at high temperature in the molten glass system, playing the role of the reducing agent. The surface tension of the molten glass coating in a reducing atmosphere increases about 20% than that of the coating in an oxidation atmosphere. The increase in the surface tension can lead to the shrinkage of the surface. Thus, the molten glass can move to the surface easily, and the pores are eliminated in the process. Thus, the surface is clean after cooling. Meanwhile, the coating can prevent the titanium alloy from oxidation because the pyrolysis carbon combined with oxygen in the coating at elevated temperature.

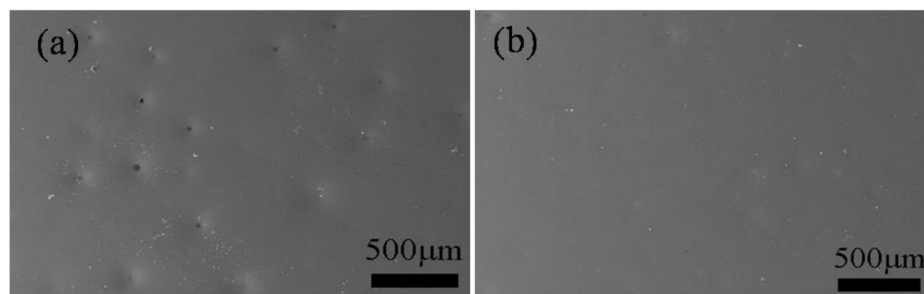


Figure 6. Surface morphologies of two kinds of glass composite coating after heating at 850 °C for 2 h: (a) the coating mixed with the WG binder; and (b) the coating mixed with the MWG binder.

3.5. Tribology Study of the Lubricant

Figure 7 shows the coefficient of friction (μ) as a function of the sliding time under unlubricated and lubricated conditions. The lubricant is the glass coating mixed with WMG binder. When the lubricant presents, the coefficient of friction stabilizes quickly at 0.30. It is noted that the coefficient of friction substantially reduced by up to 30% compared with unlubricated condition, which is due to the presence of a viscoelastic film of the molten MWG at the boundary lubricant regime [20].

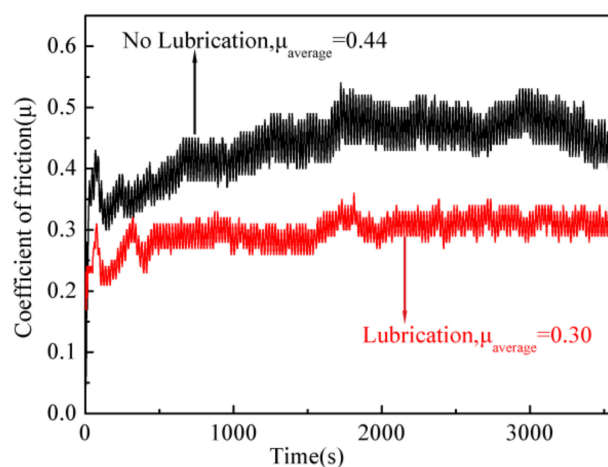


Figure 7. Coefficient of friction (μ) under unlubricated and lubricated conditions.

During the cooling period, the molten coating solidified. Then, the mismatch of the coefficient of thermal expansion (CTE) between the coating and Ti-6Al-4V alloy led to stress accumulating in the coating. The linear CTE of the glass was $1.255 \times 10^{-6}/^{\circ}\text{C}$, while that of the Ti-6Al-4V alloy was much lower ($9.7 \times 10^{-6}/^{\circ}\text{C}$). The difference of the CTE between the coating and substrate can cause cracking and flaking off from specimens due to high compressive stresses in the coating during cooling [17]. Therefore, the coating can be easily peeled off during cooling.

4. Conclusions

Sodium polyacrylate-modified sodium water glass binder was prepared successfully. The coating slurry mixed with the binder, having good suspension stability. The coating was deposited on the Ti-6Al-4V alloy surface via the slurry-dipping method. The TG-DSC analysis results of the binder showed that the total weight loss was 21.85%. When the temperature rose to 700 °C, the binder reached a stable state. The pyrolysis carbon decomposed at high temperature in the molten glass system, which played the role of the reducing agent. The reducing atmosphere increased the surface tension, which was beneficial to the shrinkage of the surface. Thus, the oxidation test performed at 850 °C in air showed the coating reduced the thickness of the oxide layer of the alloy by 51%. The coating also shows a nearly 30% reduction in the friction coefficient due to the boundary lubricant regime. During cooling, the coating can be peeled off easily because of the mismatched CTE between the coating and substrate.

Author Contributions: Shuang Yang and Dali Zhou proposed the initial work; Shuang Yang and Dali Zhou conceived and designed the experiments; Jiabei Zhou and Lei Yang provided the guidance for the experiments; Shuang Yang, Qianqian Yao and Qin Fan performed the experiments; Shuang Yang and Dali Zhou analyzed the data; Shuang Yang and Yongqiang Yang contributed reagents and analysis tools.

Conflicts of Interest: The authors declare no conflict of interest.

References

1. Li, L.X.; Rao, K.P.; Lou, Y.; Peng, D.S. A study on hot extrusion of Ti-6Al-4V using simulations and experiments. *Int. J. Mech. Sci.* **2002**, *44*, 2415–2425. [[CrossRef](#)]
2. Zhu, Y.C.; Zeng, W.D.; Ma, X.; Tai, Q.G.; Li, Z.H.; Li, X.G. Determination of the friction factor of Ti-6Al-4V titanium alloy in hot forging by means of ring-compression test using fem. *Tribol. Int.* **2011**, *44*, 2074–2080. [[CrossRef](#)]
3. Guleryuz, H.; Cimenoglu, H. Oxidation of Ti-6Al-4V alloy. *J. Alloy Compd.* **2009**, *472*, 241–246. [[CrossRef](#)]
4. Dai, J.J.; Zhu, J.Y.; Chen, C.Z.; Weng, F. High temperature oxidation behavior and research status of modifications on improving high temperature oxidation resistance of titanium alloys and titanium aluminides: A review. *J. Alloy Compd.* **2016**, *685*, 784–798. [[CrossRef](#)]
5. Li, L.X.; Peng, D.S.; Liu, J.A.; Liu, Z.Q.; Jiang, Y. An experimental study of the lubrication behavior of A5 glass lubricant by means of the ring compression test. *J. Mater. Process. Technol.* **2000**, *102*, 138–142. [[CrossRef](#)]
6. Chen, M.H.; Li, W.B.; Shen, M.L.; Zhu, S.L.; Wang, F.H. Glass-ceramic coatings on titanium alloys for high temperature oxidation protection: Oxidation kinetics and microstructure. *Corros. Sci.* **2013**, *74*, 178–186. [[CrossRef](#)]
7. Li, W.B.; Zhu, S.L.; Wang, C.; Chen, M.H.; Shen, M.L.; Wang, F.H. SiO₂-Al₂O₃-glass composite coating on Ti-6Al-4V alloy: Oxidation and interfacial reaction behavior. *Corros. Sci.* **2013**, *74*, 367–378. [[CrossRef](#)]
8. Xiao, Z.Q.; Tan, F.T.; Wang, W.; Lu, H.F.; Cai, Y.C.; Qiu, X.L.; Chen, J.G.; Qiao, X.L. Oxidation protection of commercial-purity titanium by Na₂O-CaO-SiO₂ and Na₂O-CaO-Al₂O₃-SiO₂ glass ceramic coatings. *Ceram. Int.* **2015**, *41*, 325–331. [[CrossRef](#)]
9. Sarkar, S.; Datta, S.; Das, S.; Basu, D. Oxidation protection of gamma-titanium aluminide using glass-ceramic coatings. *Surf. Coat. Technol.* **2009**, *203*, 1797–1805. [[CrossRef](#)]
10. Liu, P.; Wei, L.Q.; Ye, S.F.; Xu, H.W.; Chen, Y.F. Protecting stainless steel by glass coating during slab reheating. *Surf. Coat. Technol.* **2011**, *205*, 3582–3587. [[CrossRef](#)]

11. Moskalewicz, T.; Smeacetto, F.; Cempura, G.; Ajitdoss, L.C.; Salvo, M.; Czyrska-Filemonowicz, A. Microstructure and properties characterisation of the double layered glass–ceramic coating on near- α titanium alloy. *Surf. Coat. Technol.* **2010**, *204*, 3509–3516. [[CrossRef](#)]
12. Moskalewicz, T.; Smeacetto, F.; Czyrska-Filemonowicz, A. Microstructure, properties and oxidation behavior of the glass–ceramic based coating on near- α titanium alloy. *Surf. Coat. Technol.* **2009**, *203*, 2249–2253. [[CrossRef](#)]
13. Liang, W.; Wu, J.P.; Zhang, L. Preparation and performance of high-temperature oxidation resistant of coatings for mild carbon alloyed steel. *Geol. Sci. Technol. Inf.* **2007**, *26*, 86–90.
14. Zhang, X.J.; Gao, Y.H.; Ren, B.Y.; Tsubaki, N. Improvement of high-temperature oxidation resistance of titanium-based alloy by sol-gel method. *J. Mater. Sci.* **2010**, *45*, 1622–1628. [[CrossRef](#)]
15. Matsumoto, K.; Izawa, M.; Nakanishi, T.; Tsubouchi, K. Tribological properties of water glass lubricant for hot metalworking. *Tribol. Trans.* **2009**, *52*, 553–559. [[CrossRef](#)]
16. Schweins, R.; Huber, K. Collapse of sodium polyacrylate chains in calcium salt solutions. *Eur. Phys. J. E* **2001**, *5*, 117–126. [[CrossRef](#)]
17. Chen, G.Q.; Li, N.N.; Fu, X.S.; Zhou, W.L. Preparation and characterization of a sodium polyacrylate/sodium silicate binder used in oxidation resistant coating for titanium alloy at high temperature. *Powder Technol.* **2012**, *230*, 134–138. [[CrossRef](#)]
18. Kahlenberg, V.; Dorsam, G.; Wendschuh-Josties, M.; Fischer, R.X. The crystal structure of delta- $\text{Na}_2\text{Si}_2\text{O}_5$. *J. Solid State Chem.* **1999**, *146*, 380–386. [[CrossRef](#)]
19. Subasri, R.; Nafe, H. Phase evolution on heat treatment of sodium silicate water glass. *J. Non-Cryst. Solids* **2008**, *354*, 896–900. [[CrossRef](#)]
20. Tieu, A.K.; Wan, S.H.; Kong, N.; Zhu, Q.; Zhu, H.T. Excellent melt lubrication of alkali metal polyphosphate glass for high temperature applications. *RSC Adv.* **2015**, *5*, 1796–1800. [[CrossRef](#)]



© 2018 by the authors. Licensee MDPI, Basel, Switzerland. This article is an open access article distributed under the terms and conditions of the Creative Commons Attribution (CC BY) license (<http://creativecommons.org/licenses/by/4.0/>).